Anticipated synchronization in neuronal circuits unveiled by a phase-response-curve analysis

Fernanda S. Matias,[1,*] Pedro V. Carelli,[2] Claudio R. Mirasso,[3] and Mauro Copelli[2]
[1]*Instituto de Física, Universidade Federal de Alagoas, Maceió, Alagoas 57072-970, Brazil*
[2]*Departamento de Física, Universidade Federal de Pernambuco, Recife, Pernambuco 50670-901, Brazil*
[3]*Instituto de Fisica Interdisciplinar y Sistemas Complejos, IFISC (CSIC-UIB), Campus Universitat de les Illes Balears, E-07122 Palma de Mallorca, Spain*
(Received 9 March 2017; published 22 May 2017)

Anticipated synchronization (AS) is a counterintuitive behavior that has been observed in several systems. When AS occurs in a sender-receiver configuration, the latter can predict the future dynamics of the former for certain parameter values. In particular, in neuroscience AS was proposed to explain the apparent discrepancy between information flow and time lag in the cortical activity recorded in monkeys. Despite its success, a clear understanding of the mechanisms yielding AS in neuronal circuits is still missing. Here we use the well-known phase-response-curve (PRC) approach to study the prototypical sender-receiver-interneuron neuronal motif. Our aim is to better understand how the transitions between delayed to anticipated synchronization and anticipated synchronization to phase-drift regimes occur. We construct a map based on the PRC method to predict the phase-locking regimes and their stability. We find that a PRC function of two variables, accounting simultaneously for the inputs from sender and interneuron into the receiver, is essential to reproduce the numerical results obtained using a Hodgkin-Huxley model for the neurons. On the contrary, the typical approximation that considers a sum of two independent single-variable PRCs fails for intermediate to high values of the inhibitory coupling strength of the interneuron. In particular, it loses the delayed-synchronization to anticipated-synchronization transition.

DOI: 10.1103/PhysRevE.95.052410

I. INTRODUCTION

Anticipated synchronization (AS), as proposed originally by Voss [1,2], is a particular kind of lag synchronization that can occur in two unidirectionally coupled dynamical systems (sender-receiver) when the receiver is subject to a self-inhibitory feedback loop. It has been shown that a dynamical system described by the equations

$$\dot{\mathbf{s}} = \mathbf{f}(\mathbf{s}(t)),$$
$$\dot{\mathbf{r}} = \mathbf{f}(\mathbf{r}(t)) + K[\mathbf{s}(t) - \mathbf{r}(t - t_d)] \quad (1)$$

may present an AS solution given by $\mathbf{r}(t) = \mathbf{s}(t + t_d)$ [1,2]. In the counterintuitive AS regime, the receiver system can predict the future dynamics of the sender for certain parameter values. Anticipated synchronization has been found both experimentally and numerically in different fields including optics [3–5], electronic circuits [6], neuronal systems [7–13], and more [14–17]. In neuronal systems, AS was originally studied numerically by Ciszak and co-workers [7,8] using a FitzHugh-Nagumo model with diffusive coupling. Chemical synapses in a three-neuron sender-receiver-interneuron (SRI) motif were included by Matias *et al.* [9]. Using the Hodgkin-Huxley (HH) model, a transition from the more intuitive delayed-synchronization (DS) regime to the AS regime was found when changing the inhibitory conductance impinging on the receiver neuron. Recently, the ideas introduced in [9] were extended to neuronal populations [11] to explain the observations of a positive Granger causality, which means a well-defined unidirectional influence from a sender to a receiver region, accompanied by either a positive or negative phase lag in the recordings of the motor cortex activity of monkeys while performing a visual task [18,19]. Despite the interest attracted by AS in neuronal circuits, a thorough understanding of how this particular state is established is missing.

In this paper we use the well-known phase-response-curve (PRC; also called phase-resetting-curve) approach to gain insight into the AS regime and in particular into the DS-AS transition that occurs in the SRI motif of model neurons shown in Fig. 1(a). In the pulsatile version, PRCs describe how the spiking time of an oscillating neuron is altered by synaptic inputs. PRCs have a long history in the analysis of coupled oscillators [20]. More than 50 years ago, for instance, this technique was used to understand how excitatory and inhibitory pulses could decrease or increase firing rates of pacemaker neurons [21]. Despite its generality, the technique is particularly suitable when a neuron receives one input per cycle. As reviewed by Goel and Ermentrout [22], as well as by Canavier and Achuthan [23,24], pulsatile PRC was applied in some particular cases, namely, models of two uni- and bidirectionally coupled neurons, neurons arranged in a ring configuration, and two-dimensional and all-to-all networks. PRCs were also measured experimentally in different biological systems, from neurons [25] to circadian rhythms [26,27].

We aim at comparing the predictions from the PRC technique with numerical simulations of the SRI motif whose nodes are described by Hodgkin-Huxley neuronal models with chemical synapses. The main novelty of this study is that the PRC approach correctly predicts the existence of an AS regime, as well as the transitions from DS to AS and from AS to a phase-drift regime. Moreover, we show that in order to address the phase-locked regime when one neuron receives two inputs per cycle, a PRC function of two variables is required, whereas the usual approximation that considers a sum of two independent single-variable PRCs fails. We also show that the

*fernanda@fis.ufal.br

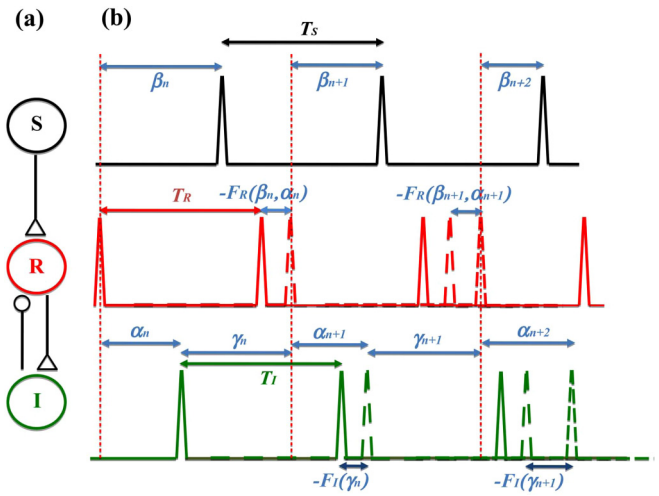

FIG. 1. (a) Three coupled neurons in a SRI configuration. Each spike of the receiver (R) is perturbed by the synaptic current from the sender (S) and the interneuron (I), whereas each spike of the interneuron is only perturbed by the synaptic current from the receiver. (b) The Poincaré map of this configuration provides the time differences between the three neurons in the phase-locking regime.

prediction of a two-variable PRC approach remains valid when the neurons in SRI motif have different free-running periods. The paper is organized as follows. The SRI motif and neuronal models are described in Sec. II. In Sec. III we develop the PRC map for this system and compare the results with the numerical integration of the full model. Finally, we summarize our results in Sec. IV.

II. THE SENDER-RECEIVER-INTERNEURON MOTIF

In the SRI motif, the sender node S projects an excitatory synapse onto the receiver node R, which also receives an inhibitory projection from the node I. Moreover, the node R projects an excitatory synapse onto node I, closing an excitatory-inhibitory loop [see Fig. 1(a)].

Each node of the motif is described by the Hodgkin-Huxley model [28], which consists of four differential equations describing the evolution of the membrane potential and the currents flowing across a patch of an axonal membrane [29]:

$$C_m\frac{dV}{dt} = \overline{G}_{\rm Na}m^3h(E_{\rm Na}-V) + \overline{G}_K n^4(E_K - V) + G_m(V_{\rm rest}-V) + I_c + \sum I_{\rm syn}, \quad (2)$$

$$\frac{dx}{dt} = a_x(V)(1-x) - b_x(V)x. \quad (3)$$

V is the membrane potential and $x \in \{h,m,n\}$ are the gating variables for sodium (h and m) and potassium (n). The capacitance of a $30\times30\times\pi$ μm^2 equipotential patch of membrane is $C_m = 9\pi$ pF. $E_{\rm Na} = 115$ mV, $E_K = -12$ mV, and $V_{\rm rest} = 10.6$ mV are the reversal potentials of the Na^+, K^+, and leakage currents, respectively. The maximal conductances are $\overline{G}_{\rm Na} = 1080\pi$ nS, $\overline{G}_K = 324\pi$ nS, and $G_m = 2.7\pi$ nS, respectively. $I_{\rm syn}$ accounts for the chemical synapses arriving from other neurons and I_c accounts for an external constant current. In the absence of synapses $I_{\rm syn} = 0$ and for $I_c = 280$ pA the neuron spikes with a period equals to $T = 14.68$ ms. The voltage-dependent rate variables in the Hodgkin-Huxley model have the forms

$$a_n(V) = \frac{10-V}{100(e^{(10-V)/10}-1)}, \quad (4)$$

$$b_n(V) = 0.125e^{-V/80}, \quad (5)$$

$$a_m(V) = \frac{25-V}{10(e^{(25-V)/10}-1)}, \quad (6)$$

$$b_m(V) = 4e^{-V/18}, \quad (7)$$

$$a_h(V) = 0.07e^{-V/20}, \quad (8)$$

$$b_h(V) = \frac{1}{(e^{(30-V)/10}+1)}, \quad (9)$$

where all voltages are measured in millivolts and the resting potential is shifted to 0 mV. All parameters are standard values from Ref. [29].

For the synapses we assumed a current-based model given by

$$I_{\rm syn}(t) = g_{\rm syn}V_{\rm syn}\sum_{\rm spikes}\alpha(t-t_{\rm spike}). \quad (10)$$

$V_{\rm syn}$ is taken, without loss of generality, equal to 1 mV. $g_{\rm syn}$ represents the maximal synaptic conductances which are different for fast excitatory synapses mediated by AMPA ($g_{\rm exc}$) and fast inhibitory synapses mediated by $GABA_A$ ($g_{\rm inh}$). The internal sum is extended over all the presynaptic spikes occurring at $t_{\rm spike}$.

The $\alpha(t)$ function that models the postsynaptic conductance is described by the following equation:

$$\alpha(t) = \pm\frac{1}{\tau_- - \tau_+}[\exp(-t/\tau_-) - \exp(-t/\tau_+)]. \quad (11)$$

The positive signal accounts for excitatory synapses, whereas the negative accounts for inhibitory ones. The parameters τ_- and τ_+ stand, respectively, for the decay and rise time of the function and determine the duration of the synaptic response. In the simulations we fix the maximum excitatory conductance $g_{\rm exc} = 1000$ nS, $\tau_- = 6.0$ ms, and $\tau_+ = 0.1$ ms.

III. RESULTS

A. Phase map

In order to apply the PRC approach to the SRI configuration shown in Fig. 1, one has to consider that the central neuron receives two inputs per cycle when locked in the 1:1 solution: one excitatory (from the sender) and another inhibitory (from the interneuron). Following the approach initially developed in Ref. [30], we define $t_R[n]$ as the spiking time at the nth cycle of the receiver, which we take as the reference to measure time differences. Let $t_S[n]$ and $t_I[n]$ be, respectively, the spiking times of the sender and interneuron immediately after $t_R[n]$ and T_S, and T_R and T_I be the free-running periods of the neurons, as shown in Fig. 1(b). To construct the return map,

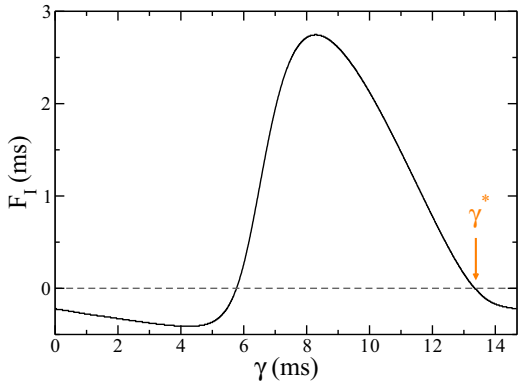

FIG. 2. Phase resetting curve for the interneuron as a function of γ [see Eq. (12)]. γ^* is the stable fixed-point solution obtained with the condition given by Eqs. (19).

we introduce the variables [depicted in Fig. 1(b)]

$$\begin{aligned}\beta_n &\equiv t_S[n] - t_R[n],\\ \gamma_n &\equiv t_R[n+1] - t_I[n],\\ \alpha_n &\equiv t_I[n] - t_R[n].\end{aligned} \tag{12}$$

From the above definitions, β_n and α_n measure, respectively, the timing of the excitatory and inhibitory inputs relative to the receiver cycle. γ_n measures the timing of the excitatory input from the receiver relative to the interneuron cycle.

The PRC of a given neuron x, F_X, is defined as the difference between its free-running period and the period after a perturbation is applied (so that positive PRCs imply period shortening). We use the synaptic function in Eq. (11) as the applied perturbation in such a way that $F_x(\delta)$ is the response due to an input $\alpha[(t-\delta)\mathrm{mod}(T_x)]$, where T_x is the free-running period of the neuron. For a periodic perturbation (with period T_p), let δ_n be the time difference between the nth spike of the neuron and the nth perturbation. The Poincaré phase map $\delta_{n+1} = \delta_n + F_x(\delta_n) + T_p - T_x$ provides the conditions for a phase-locking regime in which $\delta_{n+1} = \delta_n = \delta^*$, as described in detail in Ref. [31].

We start by analyzing the simplest case of the interneuron, whose F_I, shown in Fig. 2, depends only on the excitatory input from the receiver. From Fig. 1(b) we can start building the return map. The interval between two consecutive spikes of the I neuron satisfies

$$T_I + [-F_I(\gamma_n)] = \gamma_n + \alpha_{n+1}. \tag{13}$$

The analysis of the R neuron is more complicated, because it receives two inputs from different neurons at different times within one period. In the most general form, therefore, F_R depends on the two variables α and β that, as can be seen in Fig. 1(b), satisfy the condition

$$T_R + [-F_R(\beta_n,\alpha_n)] = \alpha_n + \gamma_n. \tag{14}$$

Isolating γ_n we get

$$\gamma_n = T_R - F_R(\beta_n,\alpha_n) - \alpha_n \equiv \gamma_n(\beta_n,\alpha_n). \tag{15}$$

This indicates that Eq. (13) can be rewritten in terms of α_n, α_{n+1}, and β_n. It is usually assumed that $F_R(\beta_n,\alpha_n)$ can be decomposed as the sum of two single-variable PRCs [23]. We will show later that this approximation fails precisely in the region of parameter space where AS occurs.

The interval between the nth spike of the receiver and the $(n+1)$th spike of the sender satisfies, as shown in Fig. 1(b),

$$\beta_n + T_S = T_R + [-F_R(\beta_n,\alpha_n)] + \beta_{n+1}. \tag{16}$$

Finally, we obtain, using Eq. (16) and combining Eqs. (13) and (15), the following two-dimensional map:

$$\beta_{n+1} = \beta_n + F_R(\beta_n,\alpha_n) + T_S - T_R, \tag{17}$$

$$\alpha_{n+1} = \alpha_n + F_R(\beta_n,\alpha_n) - F_I[\gamma_n(\beta_n,\alpha_n)] + T_I - T_R. \tag{18}$$

Two important assumptions were made here [32]. First, we assumed that the inputs affect only the following spike of each neuron, meaning that second-order effects of the PRC are neglected [23,24]. Second, we considered that the three neurons fire once in each cycle (which we know to be true from numerical integration of the equations [9]).

B. Phase-locked solutions and stability

To gain insight into the transition from anticipated to delayed synchronization (AS-DS), we look for the fixed-point solutions of Eqs. (17) and (18). We start with the case where the three neurons have the same periods.

1. *Identical free-running periods*

Assuming that the free-running periods of all three neurons are identical, $T_S = T_R = T_I = T$, the fixed-point solutions (α^*,β^*) are given by

$$\begin{aligned}F_R(\beta^*,\alpha^*) &= 0,\\ F_R(\beta^*,\alpha^*) - F_I(\gamma^*) &= 0,\end{aligned} \tag{19}$$

where $\gamma^* = \gamma_n(\alpha^*,\beta^*)$ as defined in Eq. (15). In the phase-locking regime one therefore has $F_I(\gamma^*) = 0$.

The analysis of the system of equations (19) can be done in two steps. First we find the stable fixed-point solution for the one-dimensional $F_I(\gamma^*)$ (note in Fig. 2 that the curve has two fixed points, the one with negative slope being the stable one [23,24]). Second, since Eq. (13) implies $\alpha^* = T - \gamma^*$, the search of the zero of $F_R(\alpha^*,\beta^*)$ only requires the line with constant α^* to be scanned.

In Fig. 3 we show $F_R(\beta,\alpha)$ as a function of its two arguments. This function is obtained by numerically integrating the HH equations for the R neuron subject to one excitatory and one inhibitory input at different times of the R neuron period. These two inputs are given by Eq. (11), with their appropriate parameters. For simplicity, and without loss of generality, we keep the excitatory conductance g_{exc} fixed, while we change the values of g_{inh}. The points of interest in the figure are those that satisfy $F_R = 0$. In order to find the stable fixed-point solutions of Eqs. (19), we should scan the values of the PRC in a vertical line in Fig. 3 corresponding to the stable $\alpha^* = T - \gamma^*$ value shown in Fig. 2. The stable solution is the one that crosses zero with negative slope when increasing β [filled circles in Figs. 3(a) and 3(b)]. It can be clearly seen, when comparing panels (b) and (d) in Fig. 3, that the combined effect of the two pulses is very different

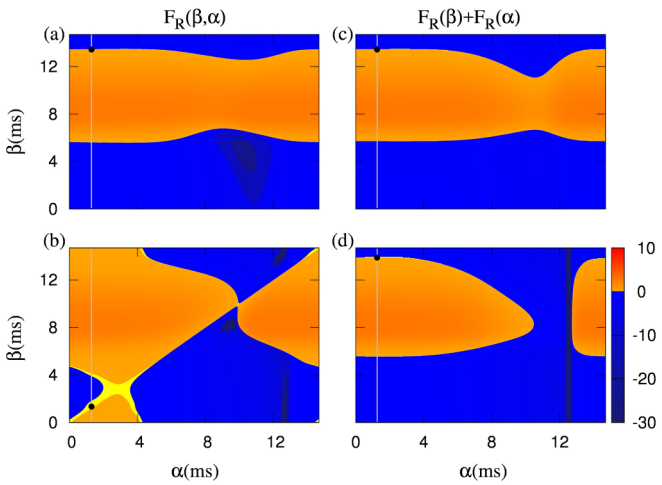

FIG. 3. Phase response curve of the receiver neuron due to two inputs per cycle. The phase response curve F_R is color-coded (in milliseconds) as a function of its two variables α and β. In (a) and (b) we plot the full function $F_R(\beta,\alpha)$, whereas in panels (c) and (d) we plot the approximation $F_R(\alpha) + F_R(\beta)$. In the upper (lower) panels, $g_{\rm inh} = 200$ nS ($g_{\rm inh} = 1000$ nS). The filled circles correspond to the stable fixed point, predicting delayed synchronization in panels (a), (c), and (d), and anticipated synchronization in panel (b). The prediction of panel (d) is incorrect (see text for details).

in the full PRC function than when we just add their effects independently.

It is worth noting that different values of the inhibitory conductance lead to severe changes in the $F_R(\beta,\alpha)$ landscape, particularly impacting the position of the fixed points relative to the pulsating period [compare Figs. 3(a) and 3(b)]. This change corresponds to a transition in the synchronization regime (from DS to AS). Let us define the spike timing difference τ_{SR} between sender and receiver (in the phase-locking regime) as the difference between their closest spikes, i.e., $\tau_{SR} = t_R - t_S$. Consequently, if $\beta^* < T/2$ [see Eqs. (12) and Fig. 1(b)], then the system is in an AS regime characterized by $\tau = -\beta^*$. On the contrary, if $\beta^* > T/2$, the system operates in the DS regime which is characterized by $\tau_{SR} = T - \beta^*$.

We now check the accuracy of the PRC prediction and compare it with the numerical simulations of the full HH model. We show in Figs. 3(a) and 3(b) two examples of $F_R(\beta,\alpha)$ for two different values of the inhibitory conductance $g_{\rm inh}$. For the parameters of Fig. 3(a) (small inhibitory conductance), the stable fixed point β^* is clearly $> T/2$ for any value of α^*. The system therefore operates in the DS regime, as long as a stable γ^* (and consequently α^*) exists.

In addition, in Fig. 3(c) we show the results when one employs the decomposition $F_R(\beta,\alpha) \approx F_R(\alpha) + F_R(\beta)$. This is the usual and simplest approximation when an oscillator receives two inputs per cycle [23,24]. In this case, $F_R(\beta)$ and $F_R(\alpha)$ represent the phase response curves of the receiver when it is subject to *either* an excitatory *or* an inhibitory input, respectively. Note that the general qualitative results of Fig. 3(c) are remarkably similar to those of Fig. 3(a). Moreover, the fixed points in both figures are almost identical. Indeed, these results predict well the stationary spiking time difference τ_{SR} directly measured in the simulations of the full Hodgkin-Huxley motif.

In Fig. 4(a) we plot the time difference τ_{SR} versus the inhibitory conductance $g_{\rm inh}$. In the numerical simulations of the full SRI motif (full circles), delayed synchronization [$\tau_{SR} > 0$; see time traces in Fig. 4(b)] is obtained for $g_{\rm inh} \lesssim 800$ nS, whereas beyond this value an anticipated synchronization regime takes over [$\tau_{SR} < 0$; see time traces in Fig. 4(c)]. For $g_{\rm inh} \gtrsim 1020$ nS, a phase-drift regime is reached, in which the receiver neuron fires slightly faster than the sender neuron. This means that the system lost the phase-locking regime. When compared with those of the PRC approach [filled squares in Fig. 4(a)], namely, the fixed-point solutions of Eqs. (19), results agree very well. The agreement extends for the whole $g_{\rm inh}$ range, including the second transition from AS to the phase-drift regime. Interestingly, when we approximate $F_R(\beta,\alpha)$ by $F_R(\beta) + F_R(\alpha)$, a good agreement is obtained only for relatively small $g_{\rm inh}$ [filled triangles in Fig. 4(a)].

For larger value of $g_{\rm inh}$, the nonlinear interaction between the pulses becomes more important and the approximation breaks down. It can be seen from panels (b) and (d) that the PRC landscapes are drastically different. In particular, in Fig. 3(b) the yellow region at low β values is a signature of anticipated synchronization, as also indicated in Fig. 4(d) (for large g_I values). It lies along the line $\beta = \alpha$, corresponding to the excitatory and inhibitory inputs arriving simultaneously at the receiver. This simultaneity (which had been observed numerically [9]) leading to the locked solution seems to be the key nonlinearity which is well captured by the two-variable PRC function. In Fig. 3(d), on the contrary, the approximation fails to describe the AS regime, keeping the fixed-point solution in the high-β^* range, therefore predicting delayed synchronization. This can also be seen in Fig. 4(e), by looking at the projection along a constant α^* value. With the full $F_R(\beta,\alpha)$ [Fig. 3(b)], an increasing inhibitory conductance causes the fixed point to cross the zero-lag solution and a small value of β^* is obtained, predicting an anticipated synchronization regime. This transition is also illustrated in Fig. 4(d). For even larger values of $g_{\rm inh}$, a transition to the phase-drift regime is obtained. Interestingly, the shape of $F_R(\beta,\alpha^*)$ shown in Fig. 4(d) for $g_{\rm inh} = 1200$ nS is reminiscent of that of a type-I excitable neuron, which is consistent with the absence of a locked regime.

It is interesting to note that the PRC in Fig. 3(b) shows that there can only be AS in this model if the receiver and interneuron are locked with $0 \leqslant \alpha^* \lesssim 4$ ms. If the synaptic dynamics is slower or there is an axonal conduction delay between the receiver and the interneuron, making them synchronize with a time difference larger than 4 ms, the prediction of the PRC approach is that AS would not occur.

2. *Different free-running periods*

Up to now, we focused on the DS-AS transition assuming identical free-running periods for all the neurons [9,11,13]. However, the PRC approach, as presented in Eqs. (17) and (18), allows an extension to the case of different free-running periods. Moreover, if T_R does not change, the same $F_R(\beta,\alpha)$ shown in Figs. 3(a) and 3(b) is, in principle, still valid. This, therefore, strengthens the predictive power of the PRC

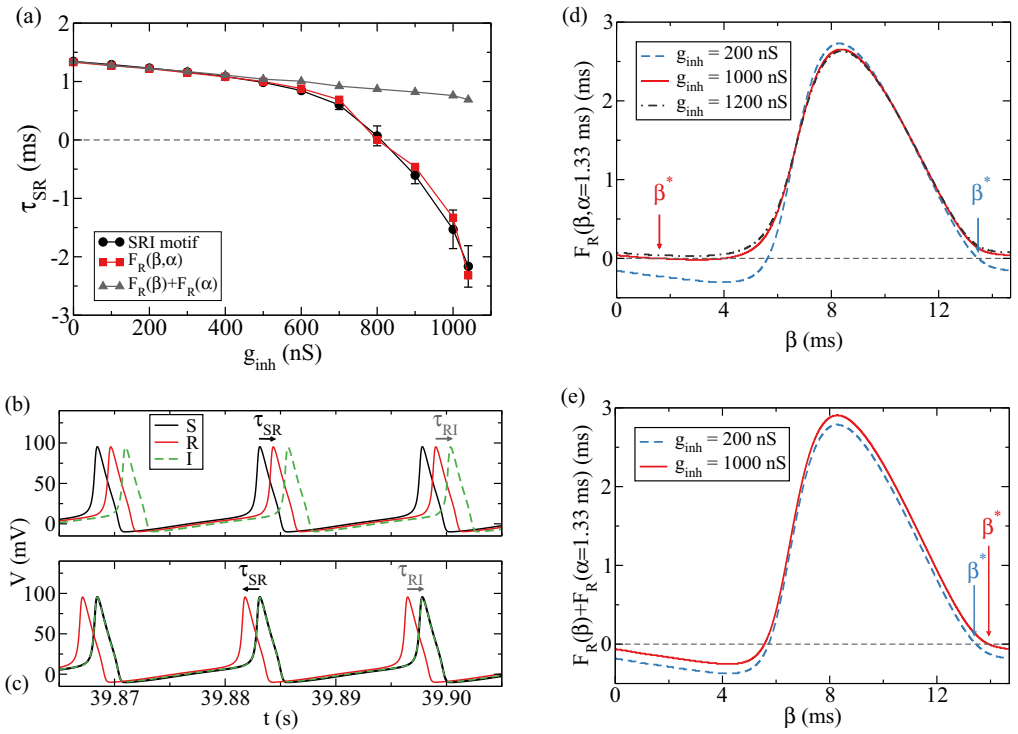

FIG. 4. Comparing numerical simulations with PRC predictions. (a) Time delay between sender and receiver as a function of the inhibitory conductance $g_{\rm inh}$. (b) and (c) Time traces of the membrane potential given by Eq. (2) for two different $g_{\rm inh}$ values: in (b) $g_{\rm inh} = 200$ nS and in (c) $g_{\rm inh} = 1000$ nS. In panel (b) the system is locked in a delayed-synchronization regime while in panel (c) it is locked in the anticipated-synchronization regime. (d) The one-dimensional $F_R(\beta,\alpha^*)$ is plotted for a fixed value of $\alpha^* = T - \gamma^*$, where γ^* is obtained from Fig. 2, for different values of $g_{\rm inh}$. (e) The one-dimensional $F_R(\beta) + F_R(\alpha^*)$ is plotted for the same value of α^* as in (d). The differences in panels (d) and (e) reflect the discrepancies in the calculations of the fixed-point solutions for β.

approach. To probe it, we analyze a particularly relevant scenario where the interneuron has a different period than the others. In neuroscience, it is often the case that inhibitory neurons spike faster than excitatory ones [31]. We therefore focus on examining the dependence of the synchronization regimes on the free-running period T_I of the interneuron.

From Eqs. (17) and (18) the fixed-point solutions for $T_S \neq T_R \neq T_I$ become

$$F_R(\beta,\alpha) = \Delta T_{RS}, \tag{20}$$

$$F_I(\gamma;T_I) = \Delta T_{IS}, \tag{21}$$

where $\Delta T_{RS} = T_R - T_S$ and $\Delta T_{IS} = T_I - T_S$.

Note that we have now included an explicit dependence of F_I on T_I. To avoid recalculating $F_I(\gamma;T_I)$ for every T_I, we use instead an approximation that assumes that changes in the period amounts to a simple rescaling of the corresponding phase response curve as

$$F_I(\gamma;T_I) \approx \frac{T_I}{T} F_I\left(\gamma\frac{T_I}{T};T\right), \tag{22}$$

where $F_I(\gamma;T)$ is the function shown in Fig. 2 for the case of the three neurons having identical period T.

The analysis of Eq. (21) with Eq. (22) allows discriminating two possibilities in terms of the F_I:

(i) If $T_S > T_I$ (or equivalently the sender frequency is smaller than the interneuron frequency), the fixed-point solutions exist until ΔT_{IS} reaches the minimum value of $F_I(\gamma;T_I)$. At this value the two fixed points collide and disappear and the system enters into a phase-drift regime.

(ii) If $T_I > T_S$ (or equivalently the sender frequency is higher than the interneuron frequency), the fixed-point solutions exist until ΔT_{IS} reaches the maximum of $F_I(\gamma;T_I)$. At this value the two fixed points collide and disappear and the system enters into a second phase-drift regime.

In Fig. 5 we plot the time difference between sender and receiver τ_{SR} as a function of the free-running period of the interneuron T_I. τ_{SR} is calculated with the fixed-point solutions γ^* obtained from Eq. (22) in combination with Fig. 3(b). A very good agreement can be seen when comparing the PRC's prediction with the numerical simulation of the full HH model. For values of $T_I \lesssim 14.5$ ms and $T_I \gtrsim 18.7$ ms the phase-locked solution is lost and the system enters into a phase-drift regime.

IV. CONCLUDING REMARKS

In this paper we showed that a PRC technique can predict the existence of an AS regime mediated by an inhibitory loop. We have also used a PRC approach to gain insight into the transition from delayed to anticipated synchronization and anticipated synchronization to phase-drift regime in a sender-receiver-interneuron motif. Initially we assumed identical parameters and operating conditions for the three neurons. The PRC of the receiver neuron was computed as a function of two inputs per cycle: one arriving from the sender and

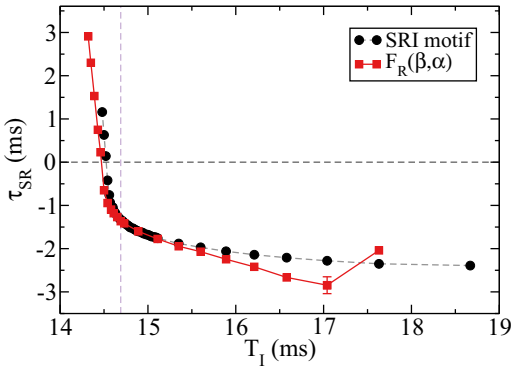

FIG. 5. Comparison between the PRC prediction and the SRI simulation for different free-running periods of the interneuron. Time delay between sender and receiver as a function of the interneuron period for the full simulation of the SRI motif (circles) and the PRC prediction (squares). The vertical dashed line corresponds to the free-running period of both the sender and the receiver. The inhibitory conductance is $g_{\text{inh}} = 1000$ nS, so that the function $F_R(\alpha,\beta)$ corresponds to that of Fig. 3(b).

another from the interneuron. We found that the description of the PRC in terms of two variables is essential to correctly match numerical results obtained from the full neuronal and synaptic model. In particular, our PRC approach correctly predicts the transition from the anticipated-synchronization to the phase-drift regime. On the contrary, if the typical approximation is used, considering the sum of two PRCs from independent stimuli, the results significantly depart from the numerical solutions, with the largest discrepancies at intermediate to large values of the inhibitory conductance. Moreover, this approximation does not account for either the AS-DS transition or the AS–phase-drift regime transition observed both numerically in the full neuronal model and with the two-variable PRC.

We have also explored the PRC prediction when the neurons had different free-running periods. Under this condition, the PRC calculation is easily extended, in particular when only the period of the interneuron element is varied. Assuming that the PRC of the interneuron modifies according to a simple rescaling factor when its period changes, we also obtain a very good agreement with the numerical simulations, highlighting the strength of the method. It is worth mentioning that anticipated synchronization is not something restricted to HH neuron models but is rather related to the characteristic of the PRC curve and the bifurcation type of the dynamical model. Further investigations including different types of synapses and neuronal models (type-I vs type-II excitability) as well as different pulsating regimes will be reported in a forthcoming publication.

ACKNOWLEDGMENTS

We thank CNPq (Grant No. 310712/2014-9), FACEPE (Grant No. APQ-0826-1.05/15), and CAPES (Grant No. PVE 88881.068077/2014-01) for financial support. C.R.M. acknowledges support from the Spanish Ministerio de Economía y Competitividad (MINECO) and Fondo Europeo de Desarrollo Regional (FEDER) through project TEC2016-80063-C3-3-R (AEI/FEDER, UE). This paper was produced as part of the activities of FAPESP Research, Innovation and Dissemination Center for Neuromathematics (Grant No. 2013/07699-0, S. Paulo Research Foundation).

[1] H. U. Voss, Phys. Rev. E **61**, 5115 (2000).
[2] H. U. Voss, Phys. Rev. Lett. **87**, 014102 (2001).
[3] C. Masoller, Phys. Rev. Lett. **86**, 2782 (2001).
[4] Y. Liu, Y. Takiguchi, P. Davis, T. Aida, S. Saito, and J. M. Liu, Appl. Phys. Lett. **80**, 4306 (2002).
[5] S. Tang and J. M. Liu, Phys. Rev. Lett. **90**, 194101 (2003).
[6] H. U. Voss, Int. J. Bifurcation Chaos Appl. Sci. Eng. **12**, 1619 (2002).
[7] M. Ciszak, O. Calvo, C. Masoller, C. R. Mirasso, and R. Toral, Phys. Rev. Lett. **90**, 204102 (2003).
[8] R. Toral, C. Masoller, C. R. Mirasso, M. Ciszak, and O. Calvo, Physica A **325**, 192 (2003).
[9] F. S. Matias, P. V. Carelli, C. R. Mirasso, and M. Copelli, Phys. Rev. E **84**, 021922 (2011).
[10] T. Pyragienè and K. Pyragas, Nonlinear Dyn. **74**, 297 (2013).
[11] F. S. Matias, L. L. Gollo, P. V. Carelli, S. L. Bressler, M. Copelli, and C. R. Mirasso, NeuroImage **99**, 411 (2014).
[12] F. S. Matias, P. V. Carelli, C. R. Mirasso, and M. Copelli, PLoS ONE **10**, e0140504 (2015).
[13] F. S. Matias, L. L. Gollo, P. V. Carelli, C. R. Mirasso, and M. Copelli, Phys. Rev. E **94**, 042411 (2016).
[14] M. Kostur, P. Hänggi, P. Talkner, and J. L. Mateos, Phys. Rev. E **72**, 036210 (2005).
[15] K. Pyragas and T. Pyragienè, Phys. Rev. E **78**, 046217 (2008).
[16] M. Ciszak, C. Mayol, C. R. Mirasso, and R. Toral, Phys. Rev. E **92**, 032911 (2015).
[17] H. U. Voss and N. Stepp, J. Comput. Neurosci. **41**, 295 (2016).
[18] A. Brovelli, M. Ding, A. Ledberg, Y. Chen, R. Nakamura, and S. L. Bressler, Proc. Natl. Acad. Sci. USA **101**, 9849 (2004).
[19] R. F. Salazar, N. M. Dotson, S. L. Bressler, and C. M. Gray, Science **338**, 1097 (2012).
[20] N. W. Schultheiss, A. A. Prinz, and R. J. Butera, *Phase Response Curves in Neuroscience: Theory, Experiment, and Analysis* (Springer Science & Business Media, New York, 2011).
[21] D. H. Perkel, J. H. Schulman, T. H. Bullock, G. P. Moore, and J. P. Segundo, Science **145**, 61 (1964).
[22] P. Goel and B. Ermentrout, Physica D **163**, 191 (2002).
[23] C. C. Canavier and S. Achuthan, Math. Biosci. **226**, 77 (2010).
[24] C. C. Canavier and S. Achuthan, in *Phase Response Curves in Neuroscience: Theory, Experiment, and Analysis* (Springer Science & Business Media, New York, 2011), Chap. 4, pp. 73–91.
[25] R. F. Galán, G. B. Ermentrout, and N. N. Urban, Phys. Rev. Lett. **94**, 158101 (2005).
[26] C. A. Czeisler, J. S. Allan, S. H. Strogatz, J. M. Ronda, R. Sanchez, C. Rios, W. O. Freitag, G. S. Richardson, and R. E. Kronauer, Science **233**, 667 (1986).
[27] S. H. Strogatz, J. Biol. Rhythms **5**, 169 (1990).

[28] A. L. Hodgkin and A. F. Huxley, J. Physiol. **117**, 500 (1952).
[29] C. Koch, *Biophysics of Computation* (Oxford University Press, New York, 1999).
[30] F. S. Matias, Ph.D. thesis, Universidade Federal de Pernambuco, 2014.
[31] E. M. Izhikevich, *Dynamical Systems in Neuroscience* (MIT Press, Cambridge, MA, 2007).
[32] T. I. Netoff, M. I. Banks, A. D. Dorval, C. D. Acker, J. S. Haas, N. Kopell, and J. A. White, J. Neurophysiol. **93**, 1197 (2005).